



ELSEVIER

Deep-Sea Research II 51 (2004) 3009–3028

DEEP-SEA RESEARCH  
PART II

[www.elsevier.com/locate/dsr2](http://www.elsevier.com/locate/dsr2)

# Spatial structure of anticyclonic eddies in the Algerian basin (Mediterranean Sea) analyzed using the Okubo–Weiss parameter

Jordi Isern-Fontanet<sup>a,\*</sup>, Jordi Font<sup>a</sup>, Emilio García-Ladona<sup>a</sup>,  
Mikhail Emelianov<sup>a</sup>, Claude Millot<sup>b</sup>, Isabelle Taupier-Letage<sup>b</sup>

<sup>a</sup>*Institut de Ciències del Mar, CMIMA-CSIC, Passeig Marítim de la Barceloneta 37-49, 08003 Barcelona, Spain*

<sup>b</sup>*Laboratoire d'Océanographie et de Biogéochimie, COM-CNRS, BP 330, 83507 La-Seyne-sur-Mer, France*

## Abstract

Three Algerian eddies (open sea big anticyclonic eddies in the Algerian basin, western Mediterranean sea) are studied in detail using altimetric and in situ data. To characterize their spatial structure we make use of the Okubo–Weiss parameter, which allows to separate the flow into vorticity-dominated and deformation-dominated regions. The application of this parameter to geostrophic velocity fields obtained from Sea Level Anomaly maps show that the observed eddies have a spatial structure in close resemblance to that found in coherent vortices of two-dimensional turbulence. These eddies appear to have a rather coherent vorticity-dominated core region surrounded by an outer region dominated by deformation with a very complicated and variable in time structure. This analysis is also applied to CTD data collected across three eddies sampled between 1997 and 1998. From these data eddy cores are equivalently defined as the interior region enclosed by the maximum of azimuthal velocity, and are consistent with the horizontal structures seen in SLA maps. The distinction between the core and the outer region (circulation cell) is particularly important to understand the role of transport and stirring of properties associated to eddies, as illustrated by the observed salinity structure, some selected SST images, and drifter trajectories. The core is characterized by very small isopycnal salinity gradients, while the surrounding cell is characterized by a strong slope of isohalines with respect to isopycnals. Persistent stagnation points are observed around the eddy and correspond to regions of high values of deformation with respect to vorticity. These regions allow analyzing characteristic patterns seen in the corresponding SST images. In addition, drifters trajectories exhibit very different behavior when crossing such regions.

© 2004 Elsevier Ltd. All rights reserved.

## 1. Introduction

Several studies have investigated the redistribution of properties in the ocean associated with intense mesoscale activity (e.g. Wilkin and

\*Corresponding author.

E-mail address: [jisern@icm.csic.es](mailto:jisern@icm.csic.es) (J. Isern-Fontanet).

Morrow, 1994; Abraham and Bowen, 2002). This intense eddy activity increases mixing in the surface layer and is mainly due to the presence of energetic and long lived structures generically named eddies (Robinson, 1983; Kamenkovich et al., 1986). In the Algerian Basin, western Mediterranean Sea, large anticyclonic open sea eddies (see Fig. 1A) have been repeatedly observed (Millot, 1985; Taupier-Letage and Millot, 1988; Benzohra and Millot, 1995b; Obaton et al., 2000; Salas et al., 2002; Ruiz et al., 2002). These mesoscale structures, named Algerian Eddies (AEs), are generated, a few times per year, as the result of an instability of the along slope Algerian current. They have variable diameters of about 100–200 km, vertical extents from 100s to 1000s of m, and can have lifetimes of several months, up to near 3 years (Millot et al., 1997; Puillat et al., 2002). The common formation and presence of these big eddies has a large impact on the surface and intermediate circulation in the western Mediterranean (Millot, 1987; Send et al., 1999; Fuda et al., 2000). They can interact with other AEs in the mid-basin, or with their parent current, sometimes leading it to be diverted seaward from the coast (Taupier-Letage and Millot, 1988; Benzohra and Millot, 1995a).

The role of these eddies on the redistribution of properties in the Algerian basin is related with the northward spreading of water mass properties that should initially be transported eastwards by the Algerian current. Evidences of a meridional momentum transport have been observed through velocities obtained from satellite Sea Level Anomaly (SLA) maps (Iudicone et al., 1998), mean climatological maps of the surface circulation (Ovchinnikov, 1966; Tziperman and Malanotte-Rizzoli, 1991) and statistical analysis of drifters (Salas et al., 2001). The signature is a meridionally enlarged and smoothed current pattern towards the central part of the Algerian basin. Similar features are observed in all climatological atlas of water properties (Picco, 1990; Brasseur et al., 1996) and in numerical simulations of the mean circulation (Herbaut et al., 1997). As an example, in Fig. 1B a mean Sea Surface Temperature (SST) image corresponding to the first semester of 1998 shows the relatively smoothed meridional gradient

of temperature to the north. This contrasts with the SST image of the Algerian basin (Fig. 1A) with complex patterns associated to three big anticyclons occupying most of the basin. The effective mixing is mainly due to the non-local transport of these eddies as they move through the whole basin (see Fig. 2 and Olson, 1991; Bouzinac et al., 1998; Puillat et al., 2002).

While theoretical and numerical simulations have shown the importance of eddies in the local dispersion of particles and their role in the evolution of tracer concentrations (e.g. Provenzale, 1999), less is known on the mixing and the stirring properties associated to these individual structures in the ocean. Dewar and Flierl (1985) analyzed with some detail the link between the stream function topology and the dispersion of a passive tracer for simple eddy models, and compared with them some features seen in SST images. In general, eddies have different dynamical properties between the inner and outer parts of their structure. While the interior part of the eddy, or core, transports tracers within it, the outer produces intense stirring of the ambient environment (Olson, 1991). Analysis of numerical results on two-dimensional turbulent flows have proposed the use of a general criterion based on the Okubo–Weiss parameter (Okubo, 1970; Weiss, 1991) to determine the detailed spatial structure of an eddy and to identify the regions with different mixing properties (McWilliams, 1984; Elhmaïdi et al., 1993).

In a previous paper (Isern-Fontanet et al., 2003) some of us have proposed to use a criterion to detect eddies from SLA maps based on the partition of the flow using the Okubo–Weiss parameter. In the present paper, we show, combining several data sets, the contribution of this criterion to understand the associated stirring properties. Data are described in Section 2 and consist on SLA maps, SST images, hydrographic measurements, and trajectories of drifters buoys. The definition of the Okubo–Weiss parameter and its application to these data are explained in detail in Section 3. The relation between stirring and mixing properties of the regions partitioned given by the parameter is analyzed in Section 4. We discuss the results and limitations of the approach

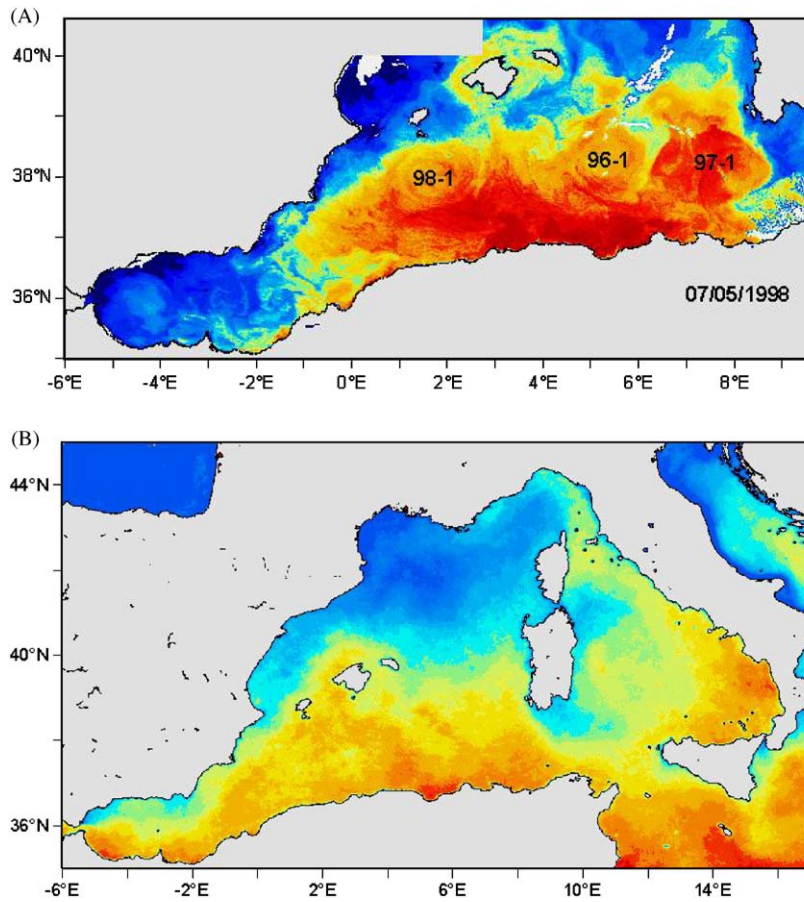


Fig. 1. (A) SST image for May 7, 1998 with the location of 96-1, 97-1 and 98-1 eddies. (B) Mean Sea Surface Temperature for the first semester of 1998. Temperature increases from blue to red, the contrast is adjusted specifically for the image to enhance the signatures of the eddies.

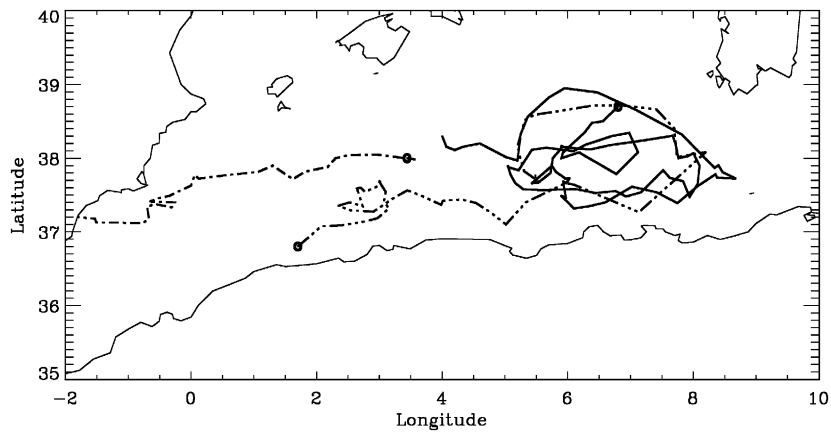


Fig. 2. Observed trajectories of 96-1 (solid line), 97-1 (dot-dot-dot-dash line) and 98-1 (dot-solid) eddies. Circles indicate the initial position observed in SLA maps. These trajectories were obtained using the methodology described in Isern-Fontanet et al. (2003).

in Section 5 and finally we summarize the main results.

## 2. Data sets

### 2.1. Satellite data

In the Mediterranean Sea, despite the weak signal intensity and the coarse space and time resolution of the altimetric tracks, several studies have shown the reliability of the altimetric data to analyze its dynamics and particularly in the Algerian basin (Vazquez-Cuervo et al., 1996; Vignudelli, 1997; Ayoub et al., 1998; Iudicone et al., 1998; Bouzinac et al., 1998; Larnicol et al., 2002; Font et al., 2004). Here we use SLA maps regularly produced by Collecte Localisation Satellites (CLS) in Toulouse, France (<http://www.cls.fr>) from a combination of both *ERS* and *TOPEX/Poseidon* altimeters measurements. These maps are processed including usual corrections (tides, inverse barometer, etc.), a Sea State empirical model with four parameters derived from a global crossover analysis (Gaspar et al., 1994) and with improved *ERS* orbits using *TOPEX/Poseidon* as a reference (AVISO User Handbook, 1996; Le Traon and Ogor, 1998). Sea level anomalies are used instead of absolute sea surface height due to the still unprecise determination of the marine geoid. SLA are regularly produced by subtracting a 4-year mean value from the actual measurements and, prior to the analysis, data are low-pass filtered using a 35 km median filter and a Lanczos filter with a cutoff wavelength of 42 km in order to reduce altimetric noise (Larnicol et al., 1995). SLA maps are finally built on a regular grid of  $0.2 \times 0.2$  degrees every 10 days using an improved space/time objective analysis method, which takes into account long wavelength errors (Le Traon et al., 1998).

The infrared satellite images used here come from the NOAA/AVHRR sensor, have been processed at the German Remote Sensing Data Center, and are freely available through its database server (<http://www.dfd.dlr.de>). Images are either processed up to SST and combined temporally to daily, weekly and monthly compo-

sites, or are plain AVHRR channel 4 of AVHRR, corresponding to relative brightness temperatures (see details on the processing in the above web site). The images here used are selected pictures to be almost simultaneous with the SLA maps. They are part of the series of images used to track eddies in the Algerian basin by Puillat et al. (2002).

### 2.2. In situ data

In connection with the EU MATER (*MASS Transfer and Ecosystem Response*) project, two field programs were carried out in the Algerian basin to study the dynamics of AEs. ELISA (*Eddies and Leddies Interdisciplinary Study in the Algerian basin*) in the eastern part (Taupier-Letage et al., 2003) and ALGERS (*the use of ERS sensors for the study of the dynamics of Atlantic water in the ALGERIAN basin*) in the western part (Font et al., 1998). Three big anticyclonic eddies, labeled 96-1, 97-1 and 98-1 (Puillat et al., 2002), were detected and sampled with CTD casts between 1997 and 1998 during ELISA1, ALGERS98 and ELISA4 cruises, respectively. These three eddies were particularly long lived and coherent structures with a clear signature in infrared images (Puillat et al., 2002; Salas, 2003) and altimetry (Isern-Fontanet et al., 2003; Font et al., 2004).

Casts during ELISA1 and ELISA4 campaigns were performed from the French RV *Le Suroit* with a SBE 911 plus CTD profiler from Sea-Bird Electronics, Inc. During the ALGERS98 campaign the CTD data were obtained from the Spanish RV *Hespérides* with a Neil Brown Mark-III probe. All data were preprocessed with the SEASOFT (v. 4.233, Sea-Bird Electronics, Inc.) software package. Final profiles were interpolated with a vertical resolution of 1 dbar. More details on data processing can be found in Ruiz et al. (2002) and Taupier-Letage et al. (2003). From all the available CTD profiles we have selected those that crossed an eddy close to one of its diameters (Fig. 3). While during ELISA4 and ALGERS98 the sections crossed completely the eddy, in ELISA1 the CTD section cut the eddy through a sector at the north and not passing close to the eddy center (Taupier-Letage et al., 2003). Cross-sections of geostrophic velocities for all the three transects were derived from

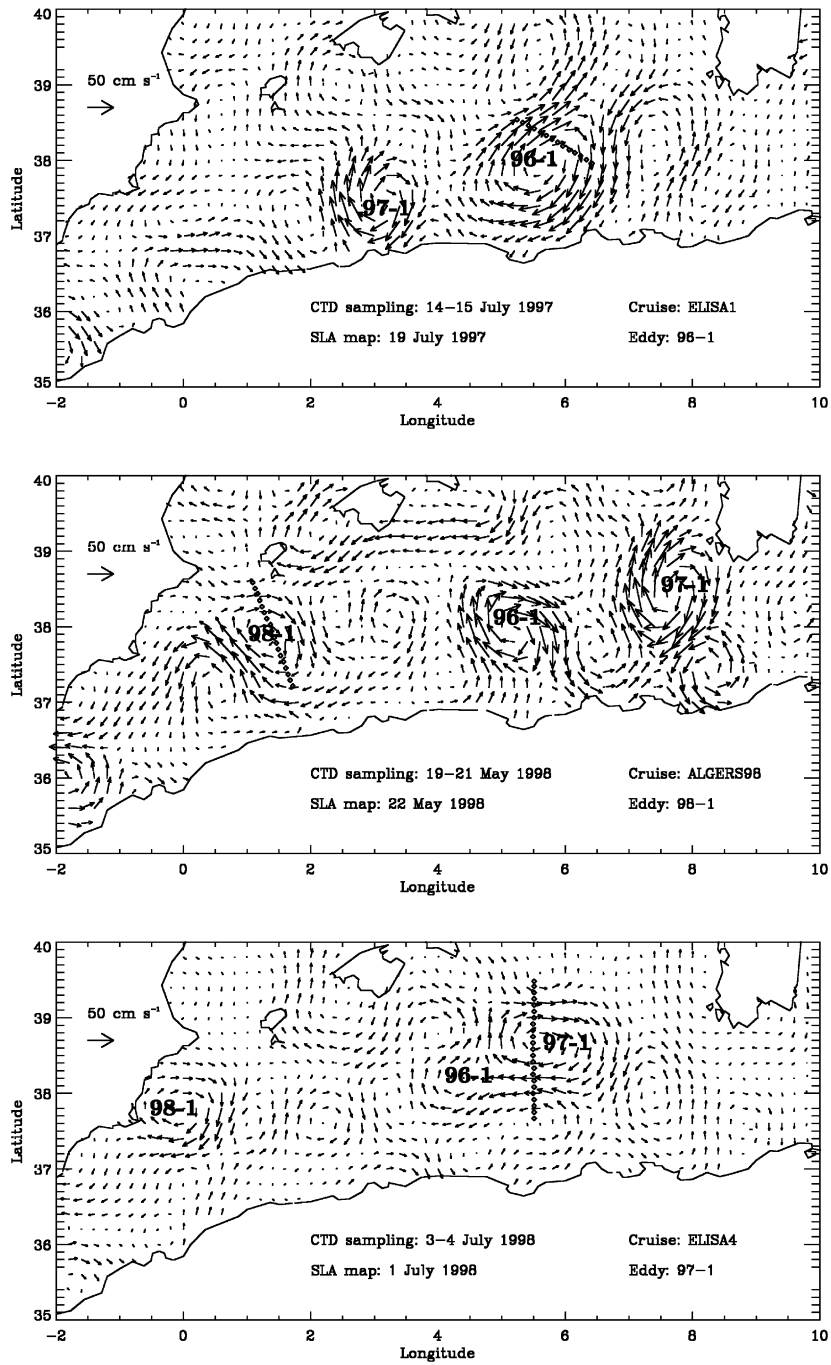


Fig. 3. Geostrophic velocities derived from SLA maps close to CTD sampling (diamonds) of eddies 96-1, 97-1 and 98-1.

dynamic heights with a reference level at 1000 dbar, similar to previous works in the region (Benzohra and Millot, 1995b). Resulting geostrophic velocities showed that the Rossby numbers for these eddies were  $Ro = 0.13$  for 96-1,  $Ro = 0.11$  for 97-1 and  $Ro = 0.09$  for 98-1. Then, the gradient flow approach was used instead of direct geostrophic velocities following Olson (1991).

In ALGERS98 cruise, 15 surface drifting buoys (drogued with a 10 m long holy sock at a mean depth of 10 m) were released across the eddy at the positions of the CTD casts (Fig. 3). The drifters were tracked during a variable number of days, from 12 to 148, until transmission stopped due to failure of the system at open sea or after having gone ashore (Salas, 2003; Font et al., 2004).

### 3. The Okubo–Weiss parameter

#### 3.1. Definition and properties

Several studies in the past have revealed the close link between the local topology of the flow field, the stirring and mixing processes, and the dispersion of Lagrangian particles in complex flows. Okubo in 1970 analyzed the dispersion in the ocean surface by looking at the shape of the trajectories of two particles initially located close to each other. By means of a linear analysis he found that the shape of the possible particle trajectories is characterized by the eigenvalues of the velocity gradient tensor. Later Weiss in 1981 arrived to an equivalent criterion analyzing the enstrophy dynamics in two-dimensional turbulent flows. In both approaches, the topology of particle trajectories and the behavior time evolution vorticity gradients is determined by the sign of

$$W = s_n^2 + s_s^2 - \omega^2, \quad (1)$$

where  $s_n$ ,  $s_s$  and  $\omega$  are the normal and the shear components of strain and the relative vorticity of the flow defined respectively by

$$s_n = \frac{\partial u}{\partial x} - \frac{\partial v}{\partial y}, \quad s_s = \frac{\partial v}{\partial x} + \frac{\partial u}{\partial y}, \quad \omega = \frac{\partial v}{\partial x} - \frac{\partial u}{\partial y}.$$

The parameter  $W$ , named after them as Okubo–Weiss parameter, allows to separate the flow into

different regions: a vorticity-dominated region ( $W < -W_0$ ), a strain-dominated region ( $W > W_0$ ) and a background field, characterized by small positive and negative values of  $W$  ( $|W| \leq W_0$ ), where  $W_0 = 0.2\sigma_W$  with  $\sigma_W$  being the standard deviation in the whole domain, in our case the Mediterranean Sea (Bracco et al., 2000; Pasquero et al., 2001). When applying this criterion of flow partition it can be observed that the general structure of an eddy consists in a vorticity-dominated inner region, the eddy core, surrounded by a strain-dominated region, the circulation cell (Elhmaïdi et al., 1993). The core edge can then be identified as the closed lines with  $W = 0$ . This separation of the field in terms of the sign of  $W$  has been proven to be a robust criterion for educing eddy cores from complex fluid flows (Jeong and Hussain, 1995; Pasquero et al., 2001; Isern-Fontanet et al., 2003). Furthermore, the boundary of the core constitutes a barrier to the exchange of particles with the surrounding cell, then particles trapped inside the eddy core remain there unless the eddy is destroyed or they are ejected through a filamentation process. In the circulation cell, on the other hand, there exist an intense stirring and exchange of particles with the background field. During the dispersion process, neutral particles exhibit a tendency to concentrate in such region (Provenzale, 1999).

For two-dimensional flow fields, as those obtained from SLA maps, the criterion is straightforward implemented by computing the velocity field and its derivatives assuming geostrophic balance

$$u = -\frac{g}{f} \frac{\partial h'}{\partial y}, \quad v = \frac{g}{f} \frac{\partial h'}{\partial x},$$

where  $h'$  is the Sea Level Anomaly,  $g$  gravity, and  $f$  the Coriolis parameter. However, for velocity transects, as those obtained from aligned CTD measurements, the criterion is not so easily implemented since it requires some assumptions on the shape of the eddy. In polar coordinates the Okubo–Weiss parameter, assuming a horizontally non-divergent flow, is given by

$$W = 4 \left[ \left( \frac{\partial v_r}{\partial r} \right)^2 + \frac{1}{r} \left( \frac{\partial v_r}{\partial \theta} \right) \left( \frac{\partial v_\theta}{\partial r} \right) - \frac{1}{r} \left( \frac{\partial v_\theta^2}{\partial r} \right) \right], \quad (2)$$

where  $v_r$  and  $v_\theta$  are the radial and azimuthal velocities,  $r$  is the radius and  $\theta$  is the azimuthal angle. A common assumption is that the eddy has axial symmetry. Then the velocity field is given by

$$v_r = 0, \quad v_\theta = V(r)$$

and then the Okubo–Weiss parameter is

$$W = -4 \frac{1}{r} \left( \frac{\partial V^2}{\partial r} \right). \quad (3)$$

This implies that the boundary of the core ( $W = 0$ ) corresponds to the radial location of the maximum of velocities. In a general case, the line of maximum kinetic energy is close to the line of  $W = 0$  but they do not necessarily coincide, as is seen from Eq. (2).

### 3.2. Satellite observations

As illustration, in Fig. 4A we have represented the horizontal distribution of  $W$  derived from a SLA map corresponding to July 7, 1996. A color scale has been selected so that blue colors represent eddy cores ( $W < -0.2\sigma_w$ ), green represents the background field ( $|W| \leq 0.2\sigma_w$ ) and yellow and red colors the deformation-dominated regions ( $W > 0.2\sigma_w$ ). When this figure is compared with a SST image (Fig. 4D) it can be observed that the core region of strong negative values of  $W$  is consistent with surface patterns labeled as 96-1, as well as the position of other eddies. One exception is the eddy located south of Mallorca island (38.5°N, 3°E) in SST image, which is not seen in the  $W$  field. However, SLA maps contain more eddy cores than those identified by visual inspection in infrared images, although it is not possible to confirm whether or not are real eddies (see Isern-Fontanet et al. (2004) for a detailed discussion). The structure of 96-1 in terms of  $W$  (Fig. 4A) displays a nearly axisymmetrical core surrounded by a region of intense deformation and irregular shape. A zonal cross-section along one of its diameters (Fig. 4B and C) shows that  $W$  (red line) takes strong negative values in the inner part (the eddy core) and becomes positive (the circulation cell) after crossing the radial position of the kinetic energy (blue line) maximum. This structure is very similar to the structure of two-dimensional vortices as those observed in turbulence (for

instance compare it with Fig. 3 of Elhmaïdi et al., 1993). To provide an evidence of the evolution of these eddies from the point of view of  $W$ , Figs. 5A–C show the spatial distribution of the parameter for three consecutive SLA maps close to ELISA1 cruise. It can be appreciated that while eddy cores are rather coherent structures in both space and time the circulation cells are much more irregular in space and variable in time.

The diameter of eddy cores can be estimated from SLA by calculating the diameter of an equivalent circular core with the same area. Observations show that 96-1 has a diameter that ranges from 95 km on 9 July 1997 to 116 km on 19 July 1997, 97-1 ranges from 116 km on 1 July to 96 km on 11 July 1998 and 98-1 from 97 to 77 km. Notice, however, that the core of 97-1 was very elongated on 1 July 1998 as observed from Fig. 3. For 96-1 the northern boundary is located between CTD 31 and 32, and the southern limit is beyond the CTD casts. The limits for 97-1 are close to CTD 235 in the north and between CTD 244 and 245 in the south. For 98-1 the limits are close to CTD 5 in the north and between CTD 14 and 15 in the south.

From a sequence of maps as the one shown in Fig. 5 the trajectories of these eddies can be recovered (as explained in detail by Isern-Fontanet et al., 2003). Once identified in one map they are tracked by looking at nearby regions of strongly negative values of  $W$  in the next map. Using this method, 96-1 was first identified in SLA maps on 19/2/1996 and lived until 21/7/1998. Eddy 97-1 from 20/5/1997 until 18/9/1998 and 98-1 from 22/2/1998 until 7/11/1998. These results give lifetimes of 883, 486 and 139 days, respectively. In situ measurements were made when 96-1 was 512 days old (ELISA1), 97-1 was 410 days old (ELISA4) and 98-1 was 88 days old (ALGERS98).

### 3.3. In situ observations

The consistency between the spatial distinction between eddy regions in SLA maps as determined by  $W$ , and the characteristics of the vertical structure of these eddies, is checked by representing vertical sections of  $\sigma_t$  and gradient velocity from the CTD measurements that approximately

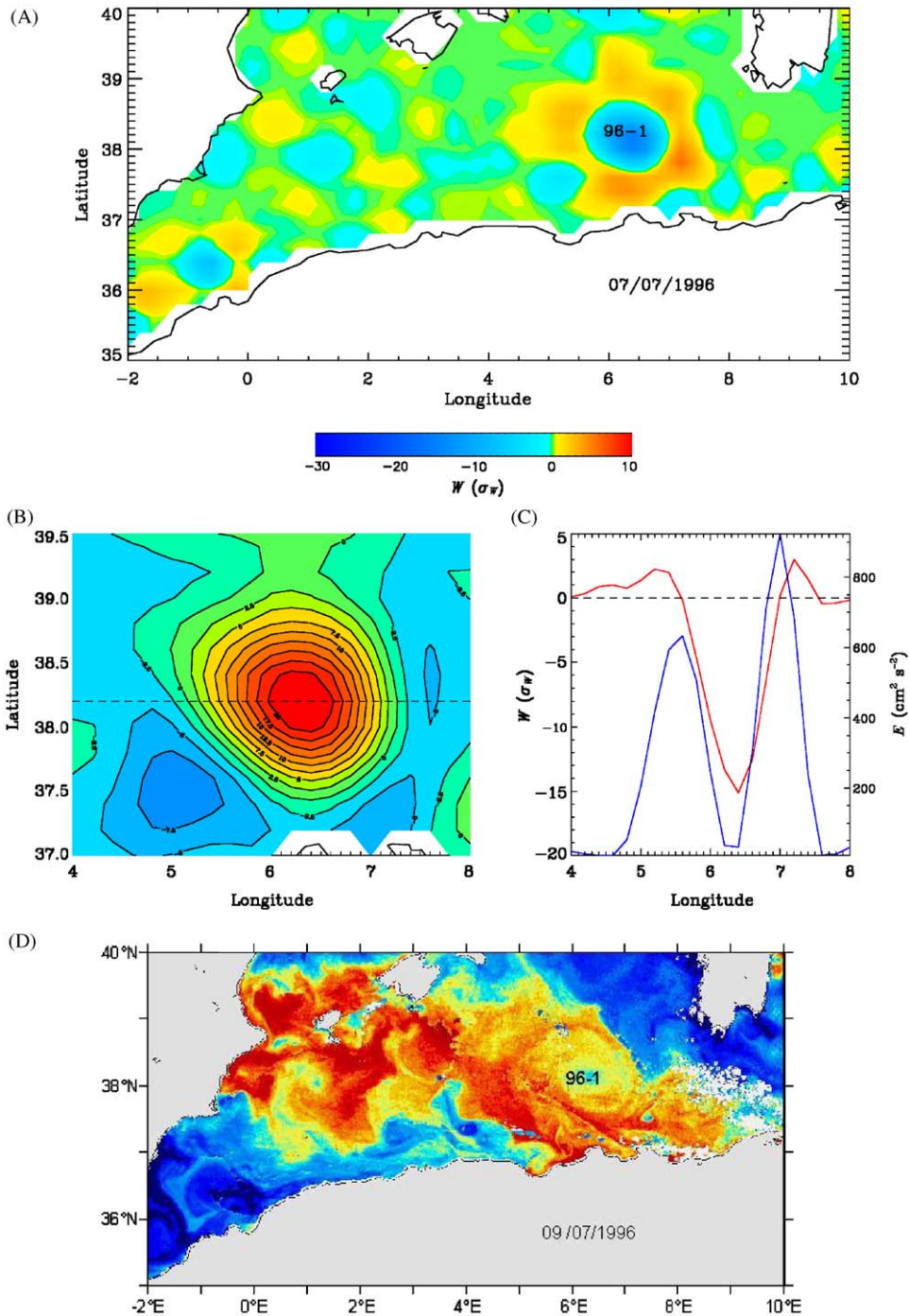


Fig. 4. The Okubo–Weiss parameter computed for the 96-1 eddy from SLA maps. (A) General view of the distribution of the Okubo–Weiss parameter on 7/7/1996. The color scale has been chosen to enhance the values above and below the line  $W = 0.2\sigma_w$  ( $\sigma_w = 2.44 \times 10^{-11}/\text{s}^2$ ). (B) Sea level anomalies (cm) corresponding to the 96-1 eddy with the transect drawn in figure C (dashed line). (C) Longitudinal profile of the Okubo–Weiss parameter (red line) and kinetic energy (blue line) across the eddy. (D) SST image corresponding to July 9, 1996. Temperature increases from blue to red, the contrast is adjusted specifically for the image to enhance the signatures of the eddies.



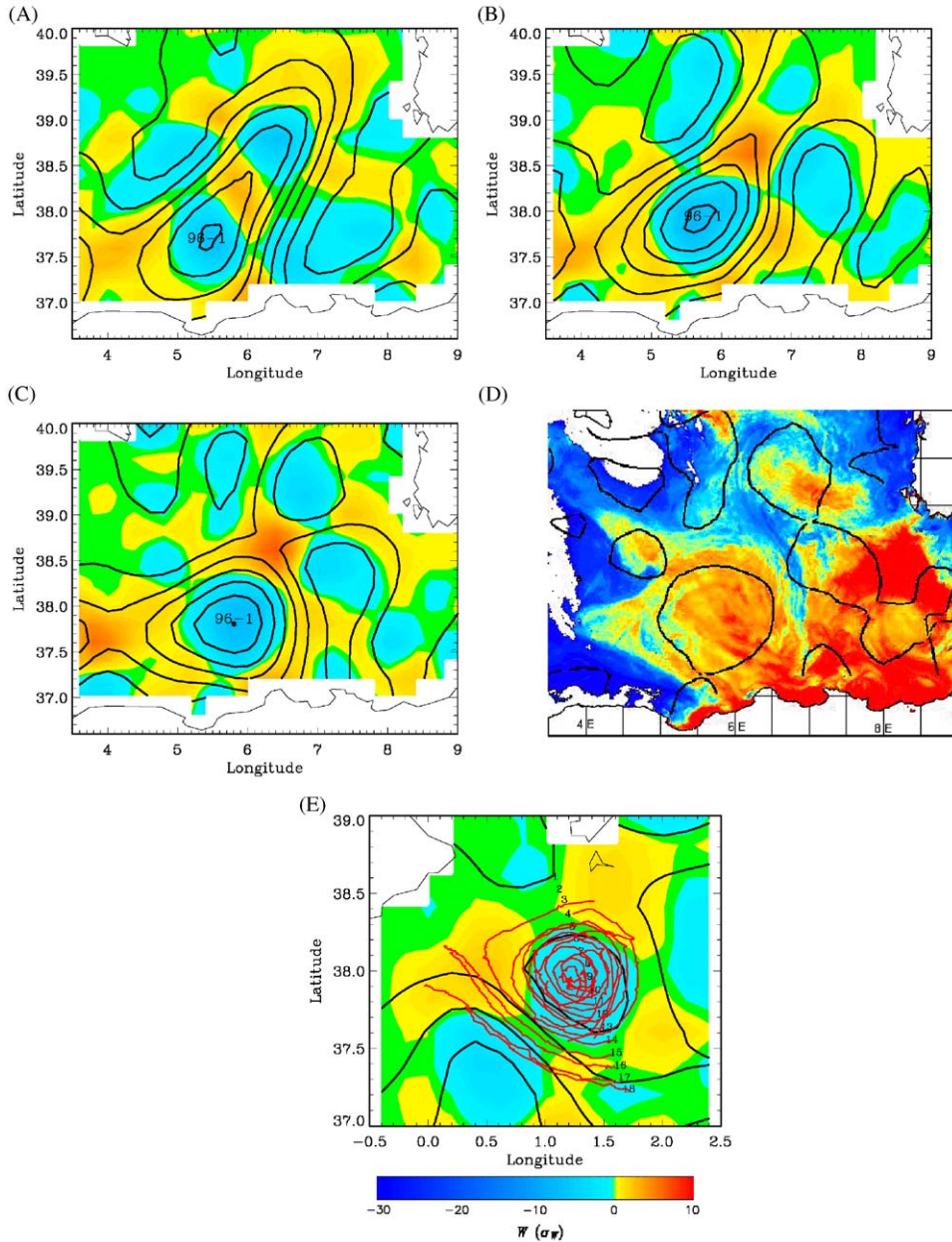


Fig. 5. Distribution of the Okubo–Weiss parameter and streaklines (black) derived from SLA maps for 96-1 close to ELISA1 cruise: (A) July 9, 1997 ( $\sigma_w = 2.64 \times 10^{-11}/s^2$ ), (B) July 19, 1997 ( $\sigma_w = 3.39 \times 10^{-11}/s^2$ ), (C) July 29, 1997 ( $\sigma_w = 3.31 \times 10^{-11}/s^2$ ). (D) SST image corresponding to July 30, 1997 with lines of  $W = 0$  (black). (E) Distribution of the Okubo–Weiss parameter and streak lines derived from SLA maps for 98-1 close to ALGERS98 cruise, May 22, 1998 ( $\sigma_w = 3.42 \times 10^{-11}/s^2$ ) and initial trajectories of drifters (red lines) launched during the cruise. Numbers indicates CTD casts. Temperature increases from blue to red, the contrast is adjusted specifically for the image to enhance the signatures of the eddies.

crossed 96-1, 97-1 and 98-1 cores (Figs. 6 and 7). The vertical structures are characteristic of anti-cyclonic eddies with the center located between casts 27–29, 237–238 and 8–10 for 96-1, 97-1 and 98-1, respectively. As expected the vertical structures are similar for both temperature and

salinity (see Ruiz et al., 2002; Taupier-Letage et al., 2003) except for the presence of a shallow thermocline located within the upper 50 m, clearly reflected in the  $\sigma_t$  sections of 96-1 and 97-1, and characteristic of the Mediterranean summer season. The vertical extent of the baroclinic structure

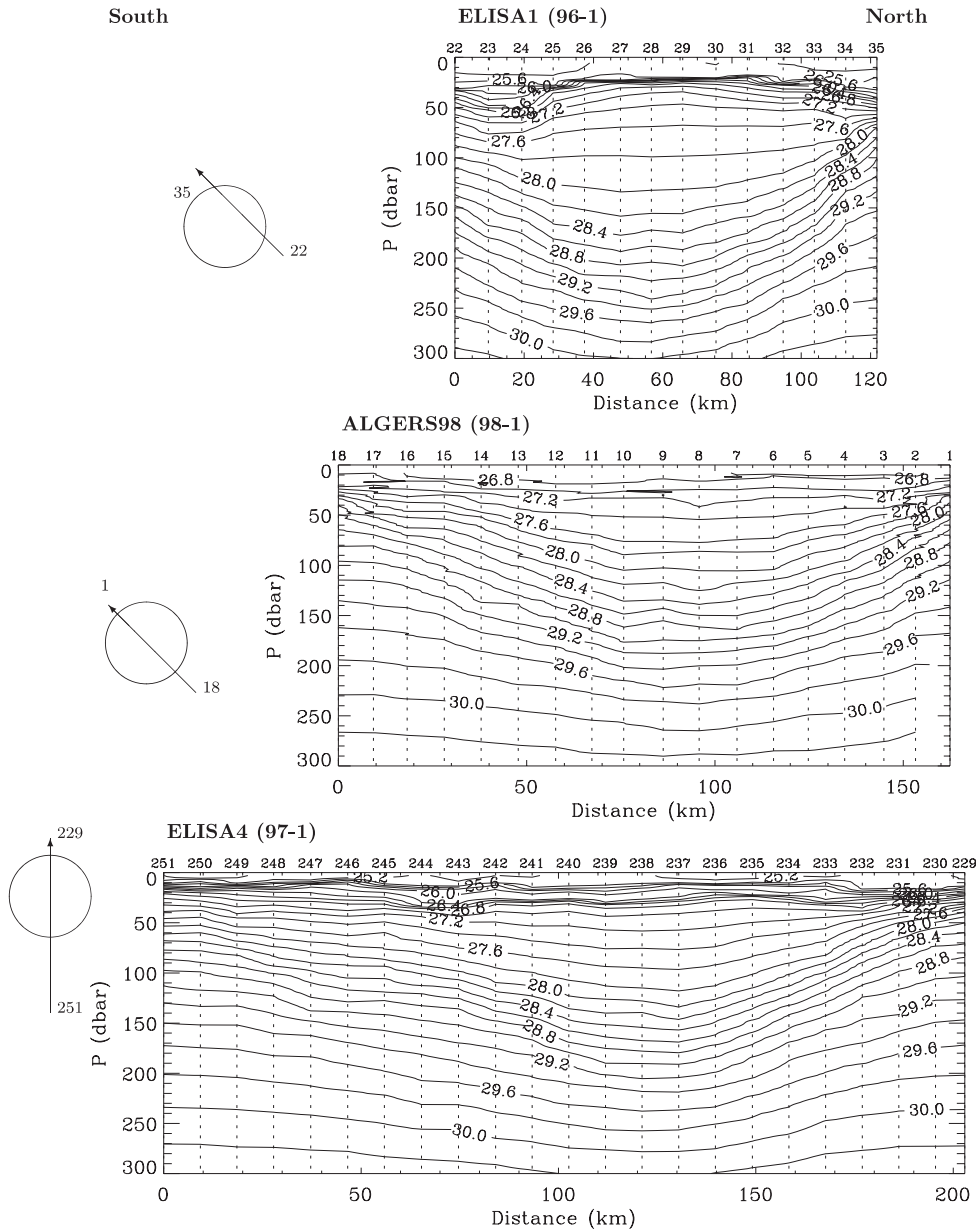


Fig. 6. Transect of  $\sigma_t$  (kg/m<sup>3</sup>) corresponding to the CTD casts shown in Fig. 3. Dotted lines are drawn at the CTD location. Numbers identify CTD casts.

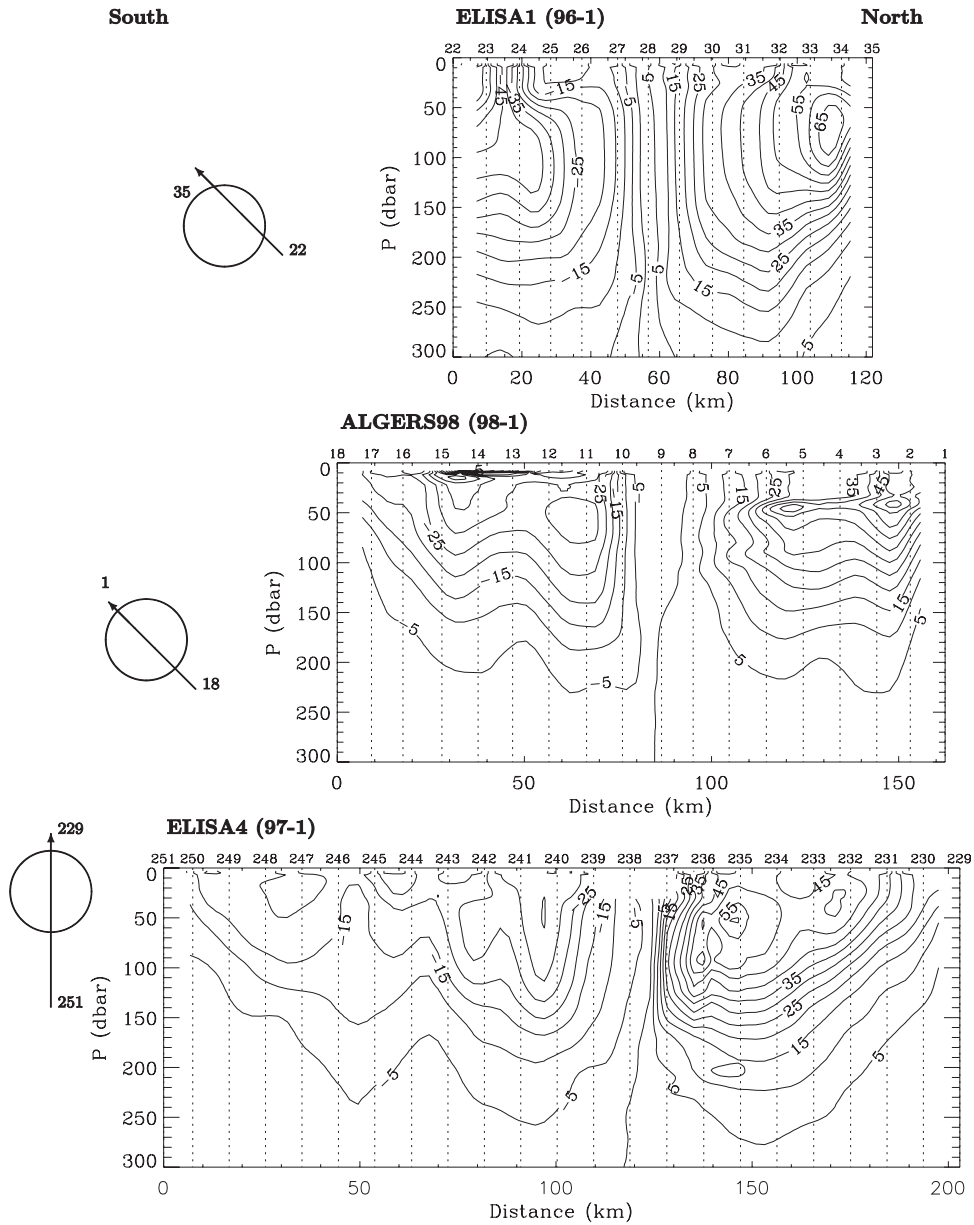


Fig. 7. Transect of the gradient flow velocities (cm/s) corresponding to Fig. 3.

is about 250–300 m and very similar for the three eddies. Gradient velocities around 50–60 cm/s can be found in the upper part, while velocities are lower than 5 cm/s below 300 m depth. For 96-1 the spatial distribution is rather symmetric with a well defined velocity extreme in the north (between

casts 33 and 34, Fig. 7) around 65 cm/s. In the south the velocity extreme was not sampled although a relative maximum can be observed around cast 24. As pointed before, some experimental evidences confirm that this CTD section was shifted to the north from the center of the

eddy structure (Taupier-Letage et al., 2003). Instead, the sections through 97-1 and 98-1 seem to capture the full horizontal extension of the eddies. Furthermore, CTD sampling in the southern part of both eddies is even clearly beyond their spatial extent. However, the spatial structure of these velocity sections has a certain complexity.

Eq. (3) has been applied to the gradient velocities shown in Fig. 7 and revealed that the resulting distribution of  $W$  is more complex than the one observed in SLA maps. However, since results were noisy, we restricted our analysis to the identification of core boundaries, and left a detailed analysis of the distribution of  $W$  in these eddies for a future study. As seen before, the identification of core boundaries, under the assumption of axial symmetry, reduces to the identification of velocity extrema. The application of this criterion to 96-1 (Fig. 7) shows that the northern boundary of the core changes with depth. Above 50 dbar it is located between CTD casts 32 and 33, while below it is located between 33 and 34. Below 130 dbar the core reduces its size and the boundary is located between casts 31 and 32. At the southern limit the boundary is located beyond the measurements. However, at a depth of about 100 dbar there is a relative maximum of velocities between cast 24 and 25. These results suggest that the diameter of the eddy core ranges from 104 to 65 km. The same analysis is applied to 98-1. It can be observed that the northern edge has two velocity extrema between CTD 2 and 3 and 5 and 4 for depths of 40 dbar. At the southern part of the eddy two velocity extrema can be found, one between casts 11 and 12 at a depth of 50 dbar and the other between 14 and 15 at the surface. Taking the inner maxima the eddy diameter is about 60 km while with the outer it is about 115 km. Finally, the 97-1 velocity structure is more complicated. The presence of several relative velocity maxima can be identified. In the northern part of the eddy there are two relative maxima in the upper layers, one between CTD 236 and 235 and the other between 232 and 233. In the southern limit velocity maximum is located between casts 240 and 241. This diameter ranges from 50 to 75 km.

#### 4. Relation with mixing

As previously outlined, the distribution of  $W$  allows identifying regions with different mixing properties. In particular, for an eddy the core is characterized by low radial mixing, and the circulation cell by intense stirring with surrounding waters. We analyze this here through the distribution of salinity, obtained from CTD casts, and SST images. The information provided by these variables is complemented by the drifting buoys trajectories observed during ALGERS'98.

##### 4.1. SST distribution and drifters

As shown by Dewar and Flierl (1985), in a frame moving at a constant velocity the region of particle trapping is the region enclosed by the critical streakline. Streaklines associated with a stream function  $\psi$ , representing an eddy propagating at a constant velocity  $(c_x, c_y)$ , are given by

$$\chi = \psi - c_x y + c_y x. \quad (4)$$

Dewar and Flierl (1985) applied it to simple models of eddies and to numerical simulations of a propagating eddy. They found that the trapping region is beyond the radial location of the maximum of velocities, which approximately defines the boundary of the eddy core in quasi axisymmetric flows.

The estimation of  $\chi$  is straightforward from altimetry if it is assumed that the eddy is steadily propagating. We have estimated the velocity of the eddy from two sequential SLA maps and computed the streaklines (Figs. 5A–C). The critical streakline should contain a stagnation point located between the closed contours around the eddy core and the first non-closed open contour. For example, in Figs. 5A–C it can be appreciated an almost stationary region observed around 37.5°N, 4°E, and in Figs. 5B, C also around 38.75°N and 6.5°E. Both regions have a strong hyperbolic character because they are dominated by deformation, that is positive values of  $W$ . SST image (Fig. 5D) exhibits two interesting features. On one hand, a pattern of relatively high-temperature clearly deformed to the west with a characteristic shape similar to the critical

streakline. The end of this lobular structure coincides with the region of great deformation. On the other hand, over the area of the second saddle point at the north of the eddy, a filament-like structure of relatively cold waters penetrates to the south surrounded by warmer waters and around the eddy core region.

During ALGERS98 several surface drifters were deployed at the same positions of CTD casts (Font et al., 2004). Their trajectories are overplotted here on the  $W$  map together with streaklines (Fig. 5E). The drifters deployed between CTD 5 and 14, which correspond to the eddy core, completed at least one loop around the eddy, as well as those drifters that were deployed at the positions of CTD 4, 15 and 16. Drifters deployed at CTD 17 and 18 escaped and did not complete any loop. In the figure the critical streakline is approximately situated between casts 14 and 16. In these locations two buoys started drifting directly to the region of the saddle point characterized by high values of deformation, and then moved eastwards until completing a loop (not shown in the figure). The drifter released in 14 also did a similar initial trajectory but after passing the saddle point region continued to loop around the eddy (see Font et al., 2004 for detailed trajectories).

#### 4.2. Salinity distribution

The implications for the mixing properties associated to the core and circulation cell for such eddies can be analyzed by considering the salinity in the upper layer as a tracer. Because the motion tends to be constrained to isopycnal surfaces, the spatial partition between core and circulation cell should be more adequate in terms of isopycnic coordinates. In order to analyze the vertical cross-sections the data were interpolated to isopycnal surfaces with a separation of  $\Delta\rho = 0.05 \text{ kg/m}^3$ . A common characteristic of the three eddies is the presence of a center with salinity about 37 surrounded by saltier waters with salinity of the order of 38. The T-S diagrams of CTD casts in the center of these eddies (Fig. 8) show the isohaline nature of the eddy core down to the 27.0–27.5  $\text{kg/m}^3$  isopycnal depending on the eddy. The contrast between the less saline core with respect to the surrounding waters is particularly enhanced in

this surface layer. Below this isopycnal the salinity differences with respect to surrounding waters are smaller, making difficult to clearly distinguish between the core and the circulation cell.

Fig. 9 shows the isopycnal distribution of salinity (thick lines) corresponding to transects shown in Figs. 6 and 7. Gradient velocity (thin lines) have been overplotted in order to make easier its comparison with salinity. For 96-1, salinity distribution inside the core is homogeneous with some well radially localized low-salinity anomalies for the upper part of the eddy, above 28  $\text{kg/m}^3$ . These salinity anomalies, located around 27.5  $\text{kg/m}^3$ , are observed at both sides of the eddy (casts 31–34 and 23–24) in the inner part of the core boundary. They can also be observed in another transect (not shown) between casts 40 and 45, which suggests that they could have a toroidal structure. Unfortunately, we do not have additional data to confirm this point. On the other hand, beyond the northern velocity maximum (casts 33 and 34) there are intense gradients of salinity. In the south, there is a small salinity gradient located between casts 24 and 25 around the 28  $\text{kg/m}^3$  isopycnal. This isopycnal variation of salinity is approximately located at the position of the maximum of velocities reported above. For eddy 98-1 the low salinity layer in the core is thinner and the analysis is more difficult. However, the salinity distribution shows the presence of strong gradients to the north of the northern velocity maximum (casts 3 and 2). Between CTD 4 and 6 it seems to be some salinity gradient that would correspond to the location of the inner maximum. At the southern part of the transect the gradients seem to be stronger at the south of the extreme located between casts 12 and 11. In 97-1 core the isohalines are predominantly flat, although there is some curvature that increases with increasing radius and becomes very steep after crossing the outer velocity maxima. In such a complex geometry the situation is not clear.

## 5. Discussion

We have evidenced the close link between the local spatial structure of the marine eddies, its

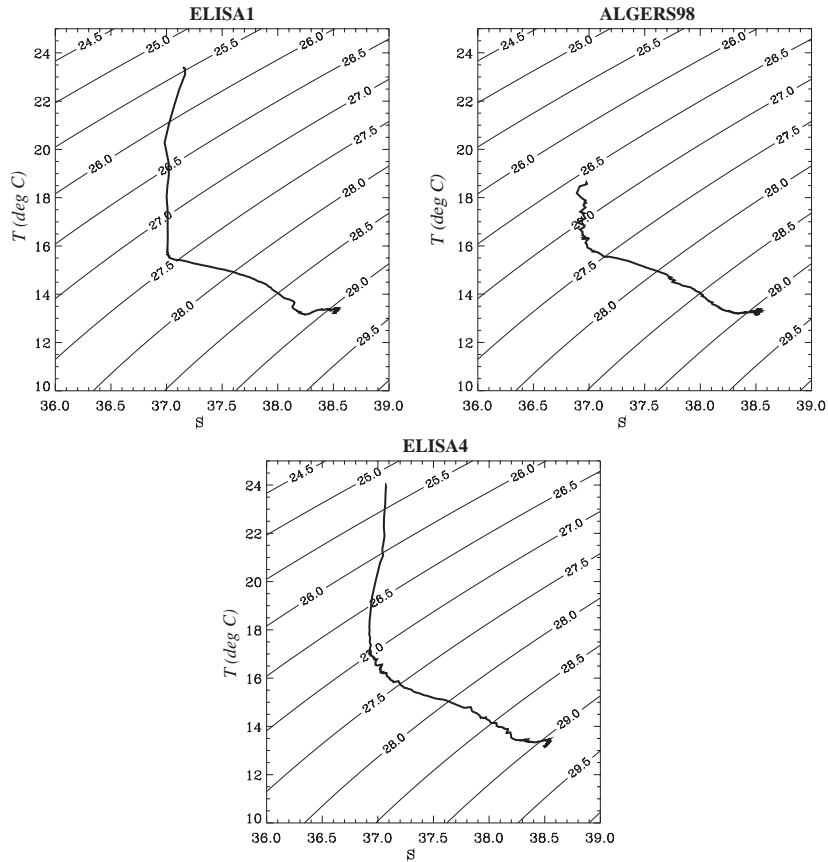


Fig. 8. T-S diagrams of the centers of eddies 96-1 (cast 27), 98-1 (cast 10) and 97-1 (cast 240). Lines of constant  $\sigma_t$  (sloping lines) are given in  $\text{kg/m}^3$ .

associated stirring properties and the spatial distribution of tracers exemplified by temperature and salinity. Unfortunately, the study is somehow restricted to find precise quantitative results essentially due to the limitations associated with the data used. Several points must be considered and discussed to evaluate the validity of the assumptions.

The basic approach to analyze the spatial structure of these eddies has been the use of  $W$  as a way to separate the different topological regions of the flow. The close resemblance of the profiles of  $W$  when an eddy is detected, and the pattern found for a vortex in two-dimensional turbulence simulations is quite remarkable (Fig. 3

in Elhmaïdi et al., 1993). This agreement between both flow fields is because, that for ocean flows at reasonably large scales, motion is almost divergenceless and tends to be constrained to isopycnal surfaces that are near horizontal. This makes it reasonable to consider a similar spatial partition applied to the flow along isopycnal surfaces. However, the flow partition in terms of straining and vorticity dominated regions, as given by the values of  $W$ , has some limitations. Two-dimensional decaying turbulence studies were proved that the validity of  $W$  is restricted to regions within eddy cores and near stagnation points (Basdevant and Philipovitch, 1994), and the partition may be rigorously addressed in

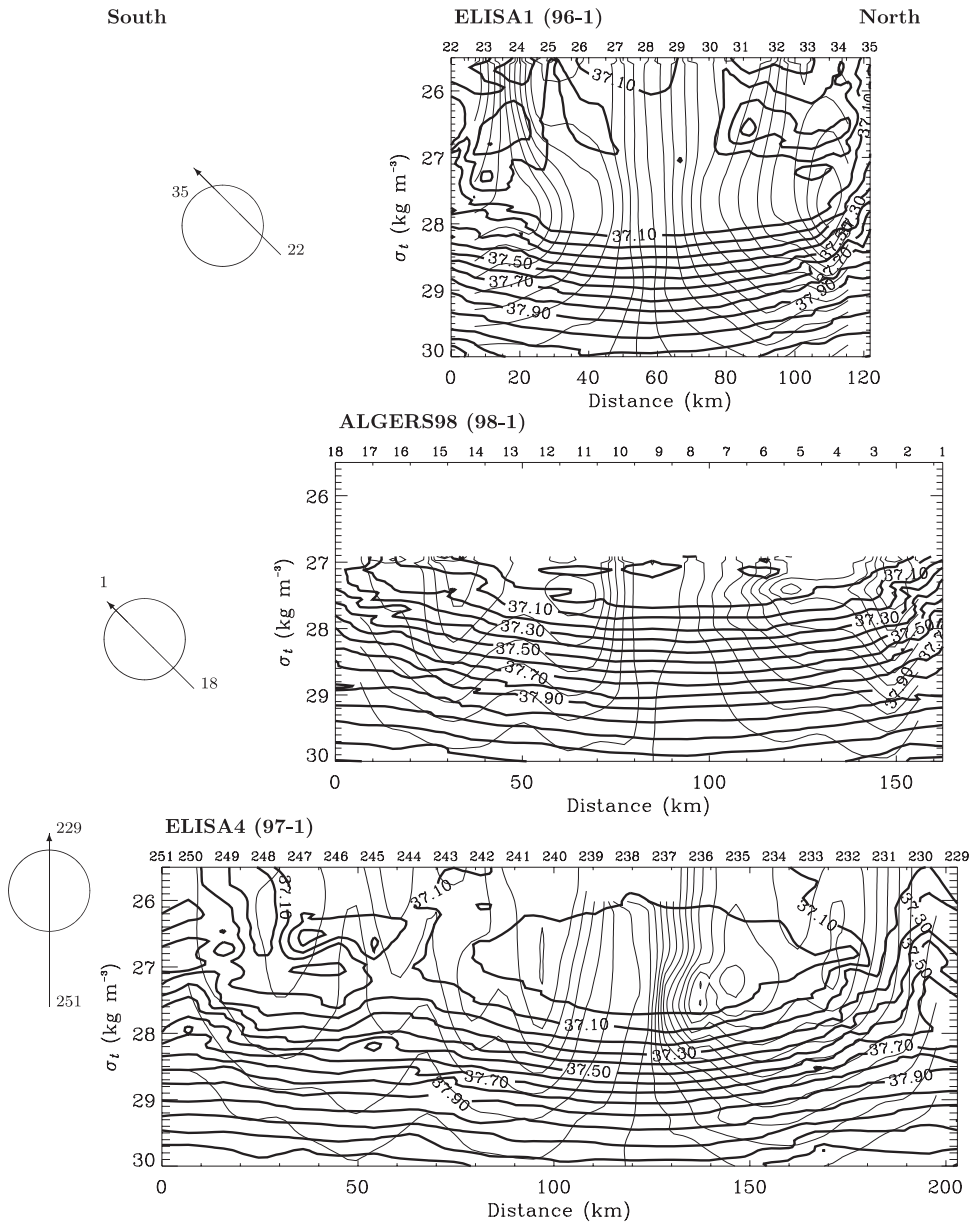


Fig. 9. Transects of salinity in isopycnal coordinates shown in Fig. 3 (thick lines) and gradient velocities (thin lines).

terms of the eigenvalues of the Lagrangian acceleration tensor (Hua and Klein, 1998). But the Okubo–Weiss separation is reasonably correct under the assumption of slowly evolving fields, which is not justified for general unsteady flows.

However, the snapshots of  $W$  distribution in the three consecutive SLA maps of for 96-1, have shown that such assumption is reasonably valid. In the last two maps (Figs. 5B and C) the eddy structure and its surrounding does not change too

much. The core is qualitatively similar in intensity, shape and location, and the two marked areas of strong deformation around it are also similar and persistent.

A second point is clearly related with the data set used in the analysis. In our opinion this is the element that mainly constraints the results presented here. Data come from several sources and devices, characterized by different resolutions in both space and time. This limits the level of description we can reach. In SLA maps the calculation of  $W$  is straightforward and it has been previously corroborated as an efficient and precise way to identify large eddies in this particular region (Isern-Fontanet et al., 2003). Problems may come from the reliability of the SLA data when constructing these maps due to the filtering and interpolation techniques. However, several comparisons between SLA maps and AVHRR data, dynamic heights and drifting buoys indicate they do not differ too much in identifying the eddies studied here. Obviously the resolution of SLA maps does not allow resolving structures as submesoscale eddies and filaments, very important to understand mixing and stirring properties (e.g. Klein et al., 1998). These can be well resolved by other remote sensing techniques with higher resolution as infrared images. Here, we have shown a close connection between the temperature patterns in one SST image and the distribution of  $W$  derived from almost simultaneous SLA maps. Nevertheless, this result is quite qualitatively, as it has been shown recently, because SST patterns reflect, not only the stirring by the flow, but also the non-conservative character of the temperature (e.g. Abraham and Bowen, 2002).

While the eddy core boundary, defined as closed lines of  $W = 0$ , does not necessarily mean a line of maximum velocity (strictly valid for axisymmetric flow), the location of this boundary, as seen by altimetry, roughly corresponds to the location of a surface velocity extremum from CTD vertical sections. However, the vertical structure of velocities is much more complex, showing in some cases (97-1) the existence of several velocity extrema that complicates the proper identification of the core boundary (Fig. 7). The resolution of

SLA maps is not enough to appreciate it because they have been filtered using a low-pass filter with cut-offs of the order of 40 km. Then, a smoothing and therefore reduction of geostrophic velocities and their gradients clearly affect the computation of  $W$  in the way of hiding the finer structure of the velocity field.

The use of salinity as a tracer has two main drawbacks. T-S diagrams of CTD data corresponding to the center of eddies show that the low salinity is constrained above the 27.5 kg/m<sup>3</sup> isopycnal, which limits the depth that can be analyzed. On the other hand, salinity is not a passive tracer since it is related to density and thus to geostrophic velocity. In any case, salinity distributions clearly indicate that the eddy core, although formed by quite homogeneous water (mainly Atlantic Water from the Algerian current, trapped when the AE was generated), is isolated from the circulation cell where water is mixed with ambient waters, then reaching characteristic values of the Mediterranean surface layer. Biological measurements in 96-1 during ELISA1 (Taupier-Letage et al., 2003) indicated the central zone was oligotrophic, as nutrients input in the surface layer associated with upwelling areas at the eddy periphery did not reach it. In 96-1 core, the quasi-homogeneous layer resulting from strong mixing during preceding spring(s) supports isolation. In the circulation cell, low-salinity filaments in the surface layer and less-mixed Levantine Intermediate Water patches support exchanges. Chlorophyll data and particulate matter distribution suggested different regimes of vertical motion associated with instability along the periphery of 96-1, while a comparison of the seston size spectra characteristics between samples in the core of 98-1 and others collected during MATER cruises in the basin indicated that the eddy was several months old with almost no exchange with surrounding waters (Rodríguez-Arias et al., 1998). It is interesting to comment the results of an experiment in which a chemical tracer was released within an eddy in the Atlantic North (Martin et al., 2001). The tracer cloud clearly evolve within the region between the center and the maximum velocity isotach. In terms of the separation given by  $W$  the tracer was released within the eddy core



region, and no exchanges were found with outer water mass.

The two distinct regions separated by  $W$ , eddy core and circulation cell, have different Lagrangian properties. The core is characterized by its impermeability to the exchange of particles with the circulation cell, which is therefore characterized by intense stirring with surrounding waters. In numerical experiments of two-dimensional turbulence it has been observed that particles in the circulation cell can be trapped for relatively long times (Elhmaïdi et al., 1993). The observation of drifters trajectories deployed during ALGERS98 cruise (Fig. 5E) shows how those deployed in a region close to the inner side of the core boundary followed closed trajectories around it. The four most external drifters moved initially very close and parallel but just arriving to the region of the stagnation point suffer an abrupt separation. Two of them escaped and the other two turned following a general path around the eddy. This separation of initially close drifters is characteristic of the critical streak line area and again consistent with the hyperbolic character of a persistent saddle point region. Recent studies on the Lagrangian properties of turbulent flows have shown that the stirring properties and their impact on tracer gradients are better studied from a Lagrangian point of view (Lapeyre et al., 2001; Haller, 2001). In general, the separation in hyperbolic and elliptic regions given by  $W$  is not equivalent with the presence of hyperbolic and elliptic Lagrangian trajectories. However, when the field is weakly unsteady a persistent region of hyperbolic character implies hyperbolic Lagrangian trajectories (Joseph and Legras, 2002).

## 6. Summary and conclusions

We have applied the Okubo–Weiss parameter,  $W$ , to analyze the spatial structure of three large mesoscale eddies in the Algerian basin. The spatial distribution of  $W$  allows distinguishing regions dominated by vorticity, eddy cores, from their surrounding regions where in general deformation dominates. Its implementation to sea level anomaly maps distinguishes quite precisely such regions

for eddies in the Algerian basin. As seen in these maps, such eddies have very coherent near axisymmetrical core regions surrounded by circulation cells variable in both time and space.

The spatial distribution of such eddy cores, in terms of the Okubo–Weiss parameter, is very similar to the coherent eddies appearing in two-dimensional turbulence studies. Assuming that motion has axial symmetry the computation of  $W$  is equivalent to finding places where the radial velocity is maximum. This assumption allows connecting roughly the horizontal structure of  $W$  of an eddy with the vertical structure of velocities computed from CTD cross sections. Besides the vertical sections contain a much noisier and rich structure than the smooth horizontal structure from SLA maps, the agreement is reasonable. Since Algerian eddies have a well-defined vertical structure with a characteristic core of a rather homogeneous salinity distribution, salinity has been used to diagnose the validity of this qualitative argument. This has been tested in the isopycnal distribution of salinity for three AEs. Results have shown that for radii greater than the radial location of the velocity maximum, isohalines have a steep slope respect to isopycnals while in the inner part they are almost parallel. So at least qualitatively, there is a good agreement between the location of the maximum of velocities and the distribution of salinity gradients.

The spatial structure of  $W$  allows finding detailed information on the stirring properties of these eddies with implications on mixing. In the example shown, 96-1, the circulation cell contains persistent regions where deformation dominates over vorticity, high positive values of  $W$ . Such regions coincide with the position of stagnation points associated to critical streak lines. This helps to understand some thermal structures seen in SST images. In particular the stagnation regions are closely related with either a strong deformation of the thermal signature associated to the eddy and with the penetration of a filament of relative cold waters around the eddy. Such region determines the abrupt change of behavior of the Lagrangian motion of drifters deployed within the eddy. In this context, other magnitudes that characterize the Lagrangian dispersion, as Liapunov

exponents, are better to establish the local dispersion and to define kinematic boundaries or transport barriers associated to flow structures (Boffetta et al., 2001). These ideas have been recently applied in the atmosphere to study the mixing and exchanges through the limits of the Antarctic polar vortex (Joseph and Legras, 2002; Koh and Legras, 2002). Unfortunately, similar analysis cannot easily be implemented with our available data and are left for the future.

In summary, despite all the theoretical limitations the results presented here show the valuable character of the diagnose based on the Okubo–Weiss parameter, first to analyze and therefore understand sea surface patterns associated to marine eddies and second as a rather approximate method to diagnose the mixing and stirring properties from available Eulerian measurements.

### Acknowledgements

This is a contribution to ELISA and ALGERS experiments and to the IMAGEN project funded by the Spanish R + D Plan (REN2001-0802-C02-02). Jordi Isern-Fontanet has been partially supported by contracts from GRAC (2FD97-0588) and IMAGEN projects. Altimetric maps for the period analyzed were elaborated and provided by CLS (Toulouse, France) under contract of the MATER project funded by the European Commission (MAS3-CT96-0051). ELISA1, ELISA4 and ALGERS98 were also partially funded by MATER. We would like to thank two anonymous reviewers for the comments that helped to improve the manuscript.

### References

- Abraham, E., Bowen, M., 2002. Chaotic stirring by a mesoscale surface-ocean flow. *Chaos* 12, 373–381.
- AVISO User Handbook, 1996. Corrected Sea Surface Heights Products, 2.0 edition. AVI-NT-011-311-CN.
- Ayoub, N., Le Traon, P., De Mey, P., 1998. A description of the Mediterranean surface variable circulation from combined ERS-1 and TOPEX/POSEIDON altimetric data. *Journal of Marine Systems* 18, 3–40.
- Basdevant, C., Philipovitch, T., 1994. On the validity of the “Weiss criterion” in two-dimensional turbulence. *Physica D* 113, 17–30.
- Benzohra, M., Millot, C., 1995a. Characteristics and circulation of the surface and intermediate water masses off Algeria. *Deep-Sea Research* 42, 1803–1830.
- Benzohra, M., Millot, C., 1995b. Hydrodynamics of an open sea Algerian eddy. *Deep-Sea Research* 42, 1831–1847.
- Boffetta, G., Lacorata, G., Redaelli, G., Vulpiani, A., 2001. Detecting barriers to transport, a review of different techniques. *Physica D* 159, 58–70.
- Bouzinac, C., Vázquez, J., Font, J., 1998. CEOF analysis of ERS-1 and TOPEX/POSEIDON combined altimetric data in the region of Algerian current. *Journal of Geophysical Research* 103, 8059–8071.
- Bracco, A., LaCasce, J., Pasquero, C., Provenzale, A., 2000. The velocity distribution of barotropic turbulence. *Physics of Fluids* 12 (10), 2478–2488.
- Brasseur, P., Beckers, J.M., Brankart, J., Shoenauen, R., 1996. Seasonal temperatures and salinity fields in the Mediterranean sea, climatological analysis of a historical data set. *Deep-Sea Research* 43, 159–192.
- Dewar, W., Flierl, G., 1985. Particle trajectories and simple models of transport in coherent vortices. *Dynamics of Atmospheres and Oceans* 215–252.
- Elhmaïdi, D., Provenzale, A., Babiano, A., 1993. Elementary topology of two-dimensional turbulence from a Lagrangian viewpoint and single-particle dispersion. *Journal of Fluid Mechanics* 257, 533–558.
- Font, J., Millot, C., Salas, J., Julià, A., Chic, O., 1998. The drift of Modified Atlantic Water from the Alboran Sea to the eastern Mediterranean. *Scientia Marina* 62 (3), 211–216.
- Font, J., Isern-Fontanet, J., Salas, J., 2004. Tracking a big anticyclonic eddy in the western Mediterranean Sea. *Scientia Marina* 68 (2), 331–342.
- Fuda, J., Millot, C., Taupier-Letage, I., Send, U., Bocognano, J., 2000. XBT monitoring of a meridian section across the western Mediterranean Sea. *Deep-Sea Research I* 47, 2191–2218.
- Gaspar, P., Ogor, F., Le Traon, P.Y., Zanife, O.Z., 1994. Estimating the sea state bias for TOPEX and POSEIDON altimeters from crossover differences. *Journal of Geophysical Research* 99 (C12), 24981–24994.
- Haller, G., 2001. Lagrangian coherent structures and the rate of strain in two-dimensional turbulence. *Physics of Fluids* 13, 3365–3385.
- Herbaut, C., Martel, F., Crépon, M., 1997. A sensitivity study of the general circulation of the Western Mediterranean sea. Part II, the response to atmospheric forcing. *Journal of Physical Oceanography* 27, 2126–2145.
- Hua, B., Klein, P., 1998. An exact criterion for the stirring properties of nearly two-dimensional turbulence. *Physica D* 113, 98–110.
- Isern-Fontanet, J., García-Ladona, E., Font, J., 2003. Identification of marine eddies from altimetry. *Journal of Atmospheric and Oceanic Technology* 20, 772–778.

- Isern-Fontanet, J., García-Ladona, E., Font, J., 2004. The vortices of the Mediterranean sea: an altimetric perspective, submitted for publication.
- Iudicone, D., Santoleri, R., Marullo, S., P., G., 1998. Sea level variability and surface eddy characteristics in the Mediterranean Sea from TOPEX/POSEIDON data. *Journal of Geophysical Research* 103(C2) 2995–3011.
- Jeong, J., Hussain, F., 1995. On the identification of a vortex. *Journal of Fluid Mechanics* 285, 69–94.
- Joseph, B., Legras, B., 2002. Relation between kinematic boundaries, stirring and barriers for the Antarctic Polar Vortex. *Journal of Atmospheric Sciences* 59, 1198–1212.
- Kamenkovich, I., Koshlyakov, A., Monin, A., 1986. *Synoptic Eddies in the Ocean*. D. Reidel Publishing Co., Dordrecht.
- Klein, P., Tréguier, A., Hua, B., 1998. Quasigeostrophic stirring of thermohaline fronts. *Journal of Marine Research* 56, 589–612.
- Koh, T., Legras, B., 2002. Hyperbolic lines and the stratospheric polar vortex. *Chaos* 12 (2), 382–394.
- Lapeyre, G., Hua, B., Klein, P., 2001. Dynamics of active and passive tracers in a mesoscale turbulent flow field. *Physics of Fluids* 13, 251–264.
- Larnicol, G., Le Traon, P., Ayoub, N., De Mey, P., 1995. Mean sea level and surface circulation variability of the Mediterranean Sea from 2 years of TOPEX/POSEIDON altimetry. *Journal of Geophysical Research* 100 (C12), 385–396.
- Larnicol, G., Ayoub, N., Le Traon, P., 2002. Major changes in the Mediterranean sea level variability from 7 years of TOPEX/POSEIDON ERS-1/2 data. *Journal of Marine Systems* 33–34, 63–89.
- Le Traon, P., Ogor, F., 1998. ERS-1/2 orbit improvement using TOPEX/POSEIDON: the 2cm challenge. *Journal of Geophysical Research* 103 (C4), 8045–8057.
- Le Traon, P., Nadal, F., Ducet, N., 1998. An improved mapping method of multisatellite altimeter data. *Journal of Atmospheric and Oceanic Technology* 15, 522–534.
- Martin, A., Richards, K., Law, C., Liddicoat, M., 2001. Horizontal dispersion within an anticyclonic mesoscale eddy. *Deep-Sea Research Part II* 48, 739–755.
- McWilliams, J., 1984. The emergence of isolated coherent vortices in turbulent flow. *Journal of Fluid Mechanics* 146, 21–43.
- Millot, C., 1985. Some features of the Algerian current. *Journal of Geophysical Research* 90 (C4), 7169–7176.
- Millot, C., 1987. Circulation in the Western Mediterranean Sea. *Oceanologica Acta* 10, 143–149.
- Millot, C., Benzohra, M., Taupier-Letage, I., 1997. Circulation off Algeria inferred from the médiproduct-5 current meters. *Deep-Sea Research* 44, 1467–1495.
- Obaton, D., Millot, C., Chabert D’Hières, G., Taupier-Letage, I., 2000. The Algerian current, comparisons between in situ and laboratory data sets. *Deep-Sea Research I* 47, 2159–2190.
- Okubo, A., 1970. Horizontal dispersion of floatable particles in the vicinity of velocity singularities such as convergences. *Deep-Sea Research* 17, 445–454.
- Olson, D., 1991. Rings in the ocean. *Annual Review of Earth and Planetary Sciences* 19, 283–311.
- Ovchinnikov, I., 1966. Circulation in the surface and intermediate layers of the Mediterranean. *Oceanology* 6, 48–59.
- Pasquero, C., Provenzale, A., Babiano, A., 2001. Parametrization of dispersion in two-dimensional turbulence. *Journal of Fluid Mechanics* 439, 279–303.
- Picco, P., 1990. Climatological atlas of the western Mediterranean. Technical Report, ENEA, La Spezia.
- Provenzale, A., 1999. Transport by coherent barotropic vortices. *Annual Review of Fluid Mechanics* 31, 55–93.
- Puillat, I., Taupier-Letage, I., Millot, C., 2002. Algerian eddies lifetime can near 3 years. *Journal of Marine Systems* 31, 245–259.
- Robinson, A., 1983. *Eddies in Marine Science*. Springer, Berlin.
- Rodríguez-Arias, M., Calafat, A., Canals, M., GRC Marine Geosciences, 1998. Differences in seston size spectra between the Málaga upwelling system (Alboran sea) and anticyclonic stable eddy in the western Algerian basin. Technical Report, University of Barcelona.
- Ruiz, S., Font, J., Emelianov, M., Isern-Fontanet, J., Millot, C., Salas, J., Taupier-Letage, I., 2002. Deep structure of an open sea eddy in the Algerian Basin. *Journal of Marine Systems* 33–34, 179–195.
- Salas, J., 2003. Evolution of the open-sea eddy ALGERS’98 in the Algerian basin with Lagrangian trajectories and remote sensing observations. *Journal of Marine Systems* 43, 105–131.
- Salas, J., García-Ladona, E., Font, J., 2001. Statistical analysis of the surface circulation in the Algerian Current using Lagrangian buoys. *Journal of Marine Systems* 29, 69–85.
- Salas, J., Millot, C., Font, J., García-Ladona, E., 2002. Analysis of mesoscale phenomena in the Algerian basin from drifting buoys and infrared images. *Deep-Sea Research I* 49, 245–266.
- Send, U., Font, J., Krahnman, G., Millot, C., Rhein, M., Tintoré, J., 1999. Recent advances in studying the physical oceanography of the western Mediterranean sea. *Progress in Oceanography* 44, 37–64.
- Taupier-Letage, I., Millot, C., 1988. Surface circulation in the Algerian basin during 1984. *Oceanologica Acta* 79–85.
- Taupier-Letage, I., Puillat, I., Millot, C., Rimbault, P., 2003. Biological response to mesoscale eddies in the Algerian basin. *Journal of Geophysical Research* 108 (0), 10.1029/1999JC000117.
- Tziperman, E., Malanotte-Rizzoli, P., 1991. The climatological seasonal circulation of the Mediterranean sea. *Journal of Marine Research* 49, 411–434.
- Vazquez-Cuervo, J., Font, J., Martínez-Benjamin, J., 1996. Observations on the circulation in the Alboran sea using ERS1 altimetry and sea surface temperature data. *Journal of Physical Oceanography* 26 (8), 1426–1439.

- Vignudelli, S., 1997. Potential use of ERS-1 and Topex/Poseidon altimeters for resolving oceanographic patterns in the Algerian Basin. *Geophysical Research Letters* 24 (14), 1787–1790.
- Weiss, J., 1991. The dynamics of enstrophy transfer in two-dimensional hydrodynamics. *Physica D* 48, 273–294.
- Wilkin, J., Morrow, R., 1994. Eddy kinetic energy and momentum flux in the Southern ocean, comparisons of a global eddy-resolving model with altimeter, drifter and current-meter data. *Journal of Geophysical Research* 99 (C4), 7903–7916.